JOURNAL OF GEOPHYSICAL RESEARCH, VOL. 90, NO. B8, PAGES 6801–6816, JULY 10, 1985

Stress and Subsidence Resulting From Subsurface Fluid Withdrawal in the Epicentral Region of the 1983 Coalinga Earthquake

PAUL SEGALL

U.S. Geological Survey, Menlo Park, California

The proximity of the May 2, 1983, Coalinga earthquake to active oil fields on Anticline Ridge led to speculation that the earthquake might have been triggered by oil field operations. Elsewhere, earthquakes have been associated with pore pressure increases resulting from fluid injection and also with subsidence resulting from fluid extraction. Simple calculations show that shales, which underlie the oil producing strata, hydraulically isolate the oil field from the earthquake focal region. The large volumes of fluid extracted from the oil fields caused a 50% decline in reservoir pressures from 1938 to 1983. These observations independently rule out substantial increases in pore pressure at focal depths due to fluid injection. A theoretical method, based on Biot's constitutive theory for fluid-infiltrated elastic media, is used to evaluate the change in stresses acting in the focal region resulting from fluid extraction in the overlying oil fields. As an independent check on the method, the subsidence of the earth's surface in response to fluid withdrawal is calculated and compared with measured elevation changes of Anticline Ridge. The producing horizons are taken to be horizontal permeable layers, bounded above and below by impermeable horizons. Strains within the producing layers are related to extraction-induced changes in pore fluid mass. Contraction of the producing layers causes the free surface to subside and strains the elastic surroundings. The calculated subsidence rate of Anticline Ridge between 1933 and 1972 is 3 mm/yr, in good agreement with the measured subsidence rate of 3.3 ± 0.7 mm/yr. Calculated pore pressure changes in the deepest producing zone also compare well with observed changes in reservoir pressure. Although the shear stresses induced by extraction favor reverse slip on either the northeast or southwest dipping nodal plane, the induced normal stresses are compressive, inhibiting fault slip. The driving stress (shear stress minus frictional resistance) acting across the northeast dipping plane increased by 0.01 MPa (0.1 bar) between 4 and 9 km depth, weakly favoring slip, and decreased by half that amount at depths of 9 to 11 km, weakly inhibiting slip. The driving stress on the southwest dipping plane increased by 0.02 MPa (0.2 bar) at 10 km, slightly favoring slip. The sign and magnitude of the pore pressure and stress changes at hypocentral depths do not support the hypothesis that the earthquake was induced, although knowledge of the rate of tectonic stress accumulation is required to assess properly the significance of the extraction-induced stresses.

INTRODUCTION

The M 6.7 Coalinga earthquake of May 1983, and its early aftershocks were located along Anticline Ridge, 10 km northeast of Coalinga, California [*Reasenberg et al.*, 1983; *Eaton et al.*, 1983]. Anticline Ridge overlies two active oil fields, one of which has been under production for more than 85 years. The proximity of the main shock epicenter to active oil fields led to speculation that the earthquake might have been triggered by oil field operations. Indeed, *Bennett and Sherburne* [1983] identified the potential association of the earthquake to the nearby oil fields as one of the major questions posed by the May 2 earthquake.

Several cases of induced seismicity associated with oil fields have been reported in the literature. It is interesting to note that induced earthquakes have been related both to increased pore pressures resulting from fluid injection [*Raleigh et al.*, 1972] and to subsidence and horizontal deformation resulting from fluid extraction [*Yerkes and Castle*, 1976]. The classic case of injection-induced seismicity occurred in the Rangely, Colorado, oil field where *Raleigh et al.* [1976] showed that seismicity was correlated with periods of increased pore pressure due to fluid injection. Earthquakes empirically associated with fluid extraction occurred in the Goose Creek, Texas [*Pratt and Johnson*, 1926], and Wilmington, California [*Kovach*, 1974], oil fields. The mechanics of extraction-induced faulting and seismicity, on the other hand, are poorly understood. It is not clear, for example, whether extraction-induced earthquakes are restricted to shallow depths, or whether they occur at depths comparable to those of injection- and reservoir-induced earthquakes. It should be noted that there have been numerous studies of the effects of fluid withdrawal on land subsidence [*Geertsma*, 1966; *Gambolati*, 1972, 1974; *Gambolati and Freeze*, 1973; *Safai and Pinder*, 1980]. Several of these studies employ analytical methods quite similar to those presented here. None, however, appear to have addressed the problems of faulting and seismicity induced by deep fluid extraction.

Finally, it should be mentioned that induced seismicity is not restricted to oil fields. Injection-induced seismicity was first recognized at the Rocky Mountain Arsenal near Denver [*Healy et al.*, 1968]. There are numerous cases of earthquakes related to filling of reservoirs, including eight events of magnitude 5 or greater [*Simpson*, 1976; *Bell and Nur*, 1978].

The main purpose of this paper is to assess the effects of operations in nearby oil fields on the pore fluid pressures and stresses acting in the focal region of the Coalinga earthquake. The first two sections review the earthquake sequence, the local geology, and history of oil production. The third section addresses the possibility of altered pore fluid pressures in the focal region. In the remainder of the paper a method is developed for computing the change in stresses acting in the focal region due to fluid extraction from the shallow crust. The method is then tested against measured changes in reservoir pressure and observed subsidence rates on Anticline Ridge.

THE 1983 COALINGA EARTHQUAKE SEQUENCE

Epicenters of the main shock and aftershocks through July 1983 are illustrated in Figure 1. The aftershocks form an elon-

Paper number 5B0262.

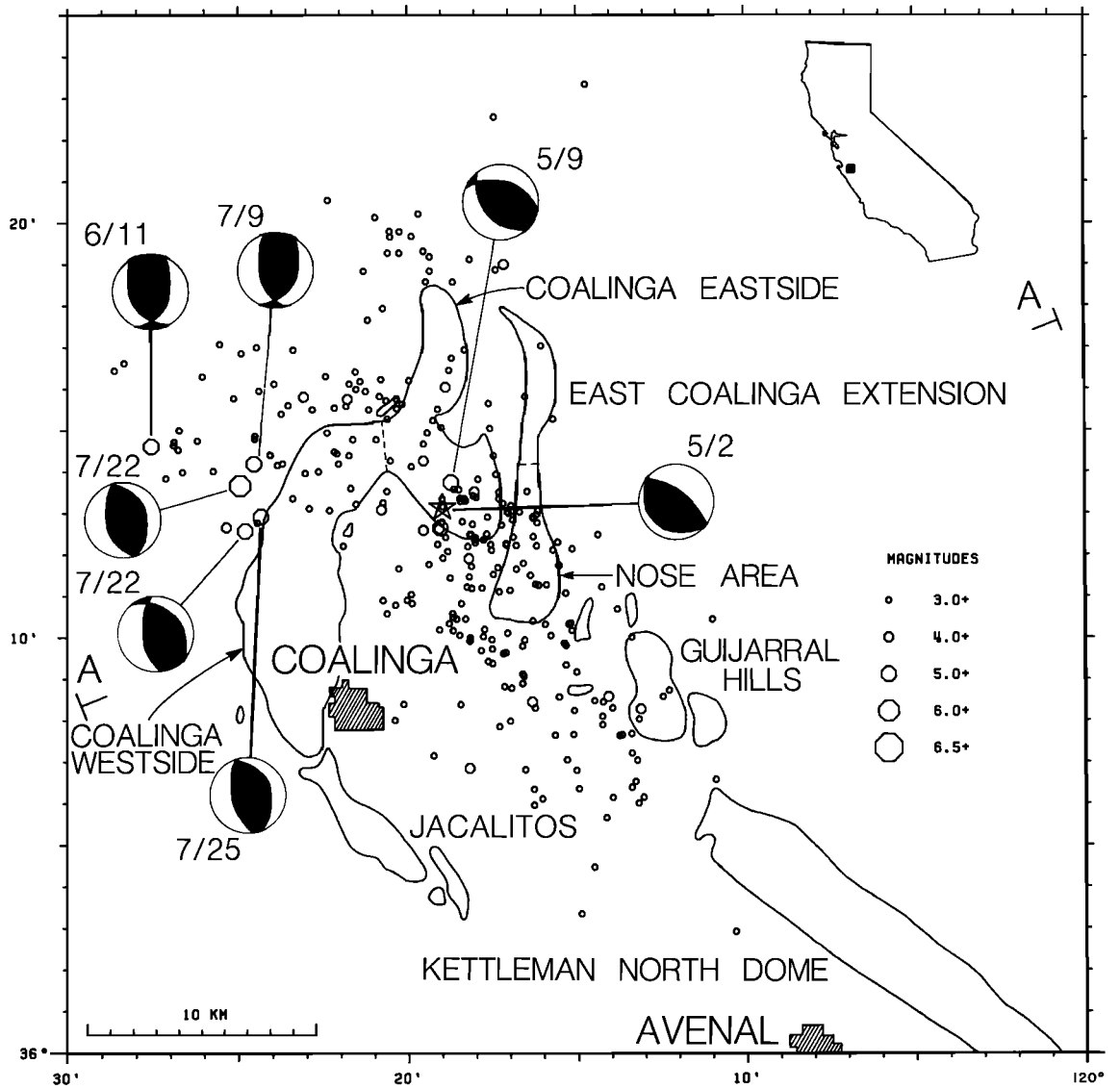

Fig. 1. Relationship between Coalinga earthquake sequence and oil fields. Main shock (star) and $M \geq 3$ aftershocks are shown for May–July 1983. Focal mechanisms are shown for $M \geq 5$ events. Outlines of the major oil fields are also shown. A-A' indicates line of cross section in Figure 2. (Seismic data are replotted from *Eaton et al.* [1983].

gate zone striking approximately N30°W, parallel to the regional trend of the Coast Ranges and the fold axis of the Coalinga anticline [*Eaton et al.*, 1983]. Figure 1 also illustrates *P* wave fault plane solutions for $M \geq 5.0$ events. The focal mechanism of the main shock indicates reverse slip on a N53°W striking fault plane which dips either 67° to the NE or 23° to the SW [*Eaton et al.*, 1983]. Coseismic elevation changes analyzed by *Stein* [1983] favor the steeply, northeast dipping plane, although the shallow plane cannot be ruled out entirely. The elevation changes can be adequately modeled by a single dislocation surface that dips 67° to the NE and extends from a depth of 4 ± 1 km to 11.2 ± 2 km [*Stein*, 1983].

On June 11, 1983, an *M* 5.2 aftershock occurred northwest of the main shock at a depth of only 4–5 km [*Eaton et al.*, 1983]. Surface rupture indicating reverse faulting on an east dipping fault was observed following this event [*Rymer et al.*, 1983]. In contrast to this, unambiguous tectonic surface ruptures were not observed following the main shock [*Clark et al.*, 1983]. During July, four $M \geq 5.0$ aftershocks occurred, including an *M* 6.4 event on July 22. All four of these events were located west of the main shock, had reverse mechanisms (Figure 1), and were located at depths of 9–10 km [*Eaton et al.*, 1983].

Geology and Oil Production of the Coalinga Region

The Coalinga area, situated between the Central Valley and the Diablo Range, is structurally dominated by northwest trending folds. The focus of the Coalinga main shock lies immediately below one such fold; the Coalinga anticline, which underlies Anticline Ridge, Guijarral Hills, and Kettleman Hills. The Pliocene and Pleistocene Tulare Formation is folded by the Coalinga anticline, attesting to the recency of deformation in the region.

Most of the historic oil production from Anticline Ridge has come from two fields, the Coalinga Eastside, and the nose area of the Coalinga East Extension (Figure 1). In the Coalinga field the principal producing horizon is the Miocene Temblor Formation. The Temblor, a pebbly sandstone, has an average thickness of 75 m and occurs at depths of 0.2–1.4 km

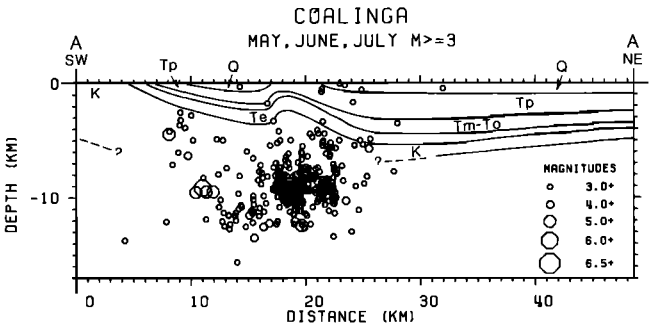

Fig. 2. Cross section of seismicity and geology. Main shock (star) and $M \geq 3$ aftershocks for May–July 1983 [after *Eaton et al.*, 1983]. Main shock and most large aftershocks have hypocentral depths near 10 km. The principal oil-producing horizons have average depths of 0.6 km (Miocene Temblor Formation) and 2.2 km (Gatchell sand, a local stratigraphic name, within Eocene strata). Q, Quaternary, Tp, Pliocene; Tm, Miocene; To, Oligocene; Te, Eocene; K, Cretaceous. Line of section illustrated in Figure 1.

(average depth of 0.6 km). It is capped by shales of the Santa Margarita Formation. The main producing zone in the Coalinga East Extension is the Gatchell sand (a local stratigraphic term) in the lower Tertiary Lodo Formation. The Gatchell is found at depths of 2.2–2.4 km in the nose area of the Coalinga anticline. The Gatchell grades into the so-called Turritella silt southwest of the Anticline Ridge, creating a strong permeability barrier to flow from the southwest. The maximum thickness of the Gatchell is 190 m.

A cross section of seismicity through Anticline Ridge (Figure 2) demonstrates that the main shock and the majority of aftershocks occurred well below the Tertiary oil-bearing formations. This is particularly true of the $M \geq 5.0$ aftershocks which, with the exception of the June 11 event, had focal depths of 9–12 km. Little is known about the geology at these depths. The deepest wells on Anticline Ridge penetrate Upper Cretaceous rocks of the Great Valley sequence, a thick section of which outcrop to the north and west of Anticline Ridge. The exposed Great Valley sequence in this region has an aggregate thickness of 8 km, nearly 5 km of which is shale [*Fowkes*, 1982]. While it is possible that the Great Valley sequence thins toward the east, seismic reflection profiles across the Coalinga anticline indicate at least 3 km of Great Valley sediments below the crest of the anticline [*Wentworth et al.*, 1984]. A conservative estimate is that at least several kilometers of argillaceous sedimentary rocks lie between the Tertiary oil-producing strata and the focus of the earthquake.

The yearly net liquid production (oil + water − returned water) from the oil fields on Anticline Ridge is shown in Figure 3. Since its discovery in 1896, 1.2×10^8 m^3 of liquid has been extracted from the Coalinga Eastside. The average extraction rate from 1905 to 1981 has been 1.6×10^6 m^3/yr or 1.0×10^7 bbl/yr. Oil production from the Coalinga East Extension did not begin until 1938, yet this field produced 1.5×10^8 m^3 of liquid. The average rate of liquid extraction from 1940 to 1981 was 3.7×10^6 m^3/yr or 2.4×10^7 bbl/yr, as indicated by the dashed line in Figure 3*b*.

Induced Fluid Pressure Changes in the Focal Region of the 1983 Earthquake

The association of induced earthquakes with active oil fields has been widely recognized since the work of *Raleigh et al.* [1972, 1976] in the Rangely oil field in western Colorado. *Raleigh et al.* [1972, 1976] proposed that fluid injection, for secondary oil recovery, increased pore pressures in the focal region of the earthquakes, thereby decreasing the effective confining stress and allowing slip to take place at the ambient levels of tectonic shear stress. It is clear then that induced pore pressure changes could have triggered the Coalinga earthquake (or any other earthquake) only if (1) oil field operations increased pore pressures in the reservoir rocks and (2) the increased fluid pressures were transmitted to the focal region of the earthquake. Neither of these conditions appear to have been met in the Coalinga area.

Records of average reservoir pressure in the Gatchell sand, the deepest producing zone within the Coalinga East Extension field at a depth of 2.2 km, have been maintained by the California State Division of Oil and Gas. The average reservoir pressure from the discovery of the field in 1938 until late 1983, following the earthquake, is shown in Figure 4. The data from 1953 to the present are average pressures, measured in between two and seven wells, within the gas zone at a depth of 1980 m. The measurements from 1938 to 1953 are from the oil zone at a depth of 2060 m. Although various secondary oil recovery projects have involved the injection of gas, water, and polymer solutions into the Gatchell, the net effect of oil field operations between 1938 and 1983 has been to reduce the

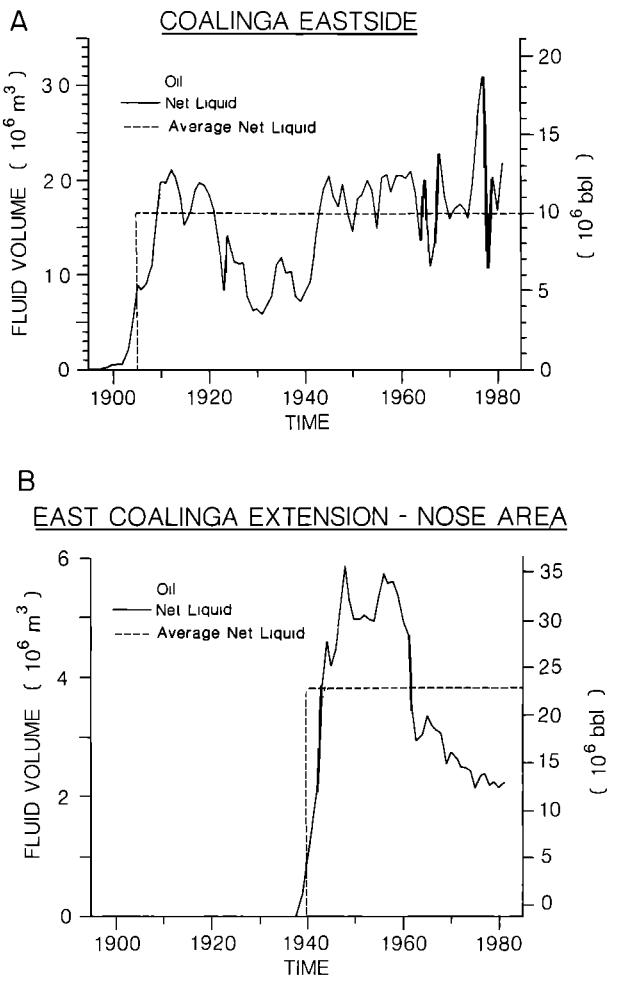

Fig. 3. Production history of Anticline Ridge oil fields. Net liquid is defined as oil + water − returned water. (*a*) Coalinga Eastside. (*b*) Coalinga East Extension, nose region (from *Conservation Committee of California Oil Producers* [1931–1984] and *California Division of Oil and Gas* [1945–1981].

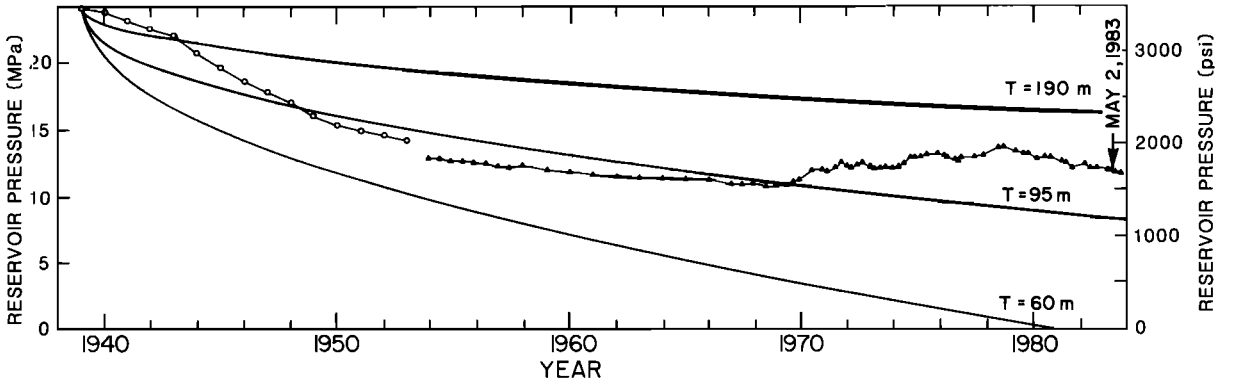

Fig. 4. Reservoir pressure with time in the Gatchell sand (a local stratigraphic name), Coalinga nose area of the Coalinga East Extension field. Circles represent pressures measured within the oil zone (2060 m); triangles are pressures measured within the gas cap (1980 m). Solid lines are calculated pressure histories assuming fluid withdrawal at a constant rate (see text). T is thickness of producing zone.

pore pressure by 53%, from 23 MPa (3500 psi) to 11 MPa (1650 psi). The pressure history is clearly dominated by the large volumes of fluid withdrawn from the reservoir. If the observed decrease in pore pressure was, in fact, transmitted to the focal region of the earthquake, it would have resulted in an increase in effective confining stress and, according to the usual criteria, a "strengthening" of the fault.

Simple calculations, however, suggest that it is extremely unlikely that any pore pressure changes within the Gatchell could have been transmitted to the focal depth of 10 km in the 45 years between 1938 and 1983. This results primarily from the low permeability of argillaceous rocks which are known to underlie the Gatchell sand. Permeabilities of shales, measured in laboratory samples and in situ [*Brace*, 1980], are typically 10^{-18} to 10^{-20} m^2 (10^{-6} to 10^{-8} darcy). For flow of water these permeabilities correspond to hydraulic diffusivities c of 10^{-5} to 10^{-7} m^2/s. Because pore fluid transport is a diffusive process, the penetration depth of a pressure disturbance at time t can be estimated by $(ct)^{1/2}$. This indicates that a pressure disturbance will penetrate 10–100 m in 45 years, two to three orders of magnitude less than the 8 km between the Gatchell and the earthquake focus. Recall that several kilometers of this section are known to consist of argillaceous Great Valley sedimentary rocks. This calculation illustrates that even a thin layer of shale hydraulically isolates the focal region from the oil fields.

It is always possible that a highly permeable fracture zone might link the oil field to the focal region, yet at present, there is no evidence to support the presence of such a zone. Even if a highly conductive zone existed, the effect of oil activities would be to decrease the pore pressure, as discussed above. In sum, all of the available evidence argues against the Coalinga earthquake having been triggered by pore pressure changes induced by diffusive transport.

On the other hand, the large volumes of fluid withdrawn from shallow, producing horizons directly above the earthquake focus raise the question of whether or not faulting was triggered by fluid extraction. The remainder of the paper attempts to evaluate this possibility by computing the change in stress acting in the focal region due to fluid extraction from the shallow crust.

PHYSICAL EFFECTS OF FLUID EXTRACTION

Stresses related to fluid extraction arise as the producing rocks contract in response to removal of pore fluid. This can be seen by considering what happens when fluid is extracted from a small volume of rock within the earth. Of course, the extraction of fluid decreases the pore pressure within the depleted volume, and this in turn drives pore fluid flow toward the volume. For the moment, however, we will consider only the immediate (undrained) changes in stress induced by extraction, before appreciable flow has taken place. This problem will be treated in some detail, primarily for the physical insight it provides. It will later be shown that the solution to the problem of localized depletion of pore fluid serves as the Green's function for the general problem of extraction-induced deformation.

Localized Depletion of Pore Fluid

The earth's crust is considered to be a uniform, isotropic, fluid-infiltrated half-space, which for simplicity will be assumed to be initially unstressed. Imagine that a small element is cut from the half-space (1 in Figure 5*a*). Because the region is unstressed, this induces no strain in the half-space. Following this, fluid with mass per unit solid volume Δm is uniformly

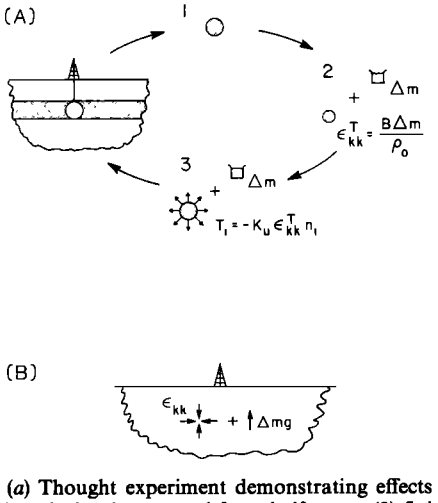

Fig. 5. (*a*) Thought experiment demonstrating effects of fluid extraction: (1) Inclusion is removed from half-space, (2) fluid with mass Δm is extracted from the inclusion, causing the inclusion to contract, and (3) applied stresses restore the inclusion to its initial shape, allowing it to be reinserted into the half-space. (*b*) The stresses in the surrounding matrix are equivalent to a (negative) point center of dilation, representing the contraction, and a vertical point force, repesenting the change in fluid mass.

extracted from the pores of the element (2 in Figure 5a). This causes the element to undergo a uniform volumetric contraction $\varepsilon_{kk}{}^T$. This "transformation strain" [*Eshelby*, 1957] occurs without induced stresses in the solid and is therefore referred to as a "stress-free strain." Because the strain resulting from uniform fluid withdrawal is purely volumetric, the strain in the element is simply

$$\varepsilon_{ij} = \varepsilon_{kk}{}^T \delta_{ij}/3 \qquad i, j, k = 1, 2, 3 \tag{1}$$

where

$$\delta_{ij} = 0 \qquad i \neq j$$

$$\delta_{ij} = 1 \qquad i = j$$

The magnitude of the transformation strain is related to the change in fluid mass content per unit volume Δm through the constitutive equations for the fluid-infiltrated solid. For a linear, isotropic, poroelastic material [*Biot*, 1941; *Rice and Cleary*, 1976] the solid strains ε_{ij} are taken to be linear functions of the solid stress σ_{ij} and fluid mass content (Appendix A, equation (A3)):

$$2\mu\varepsilon_{ij} = \sigma_{ij} - \frac{\nu_u}{1+\nu_u}\sigma_{kk}\delta_{ij} + \frac{2\mu B}{3\rho_0}\Delta m\delta_{ij} \tag{2}$$

where μ is shear modulus, ν_u is the undrained Poisson's ratio, B is Skempton's pore pressure coefficient, and ρ_0 is the reference fluid density. Undrained conditions refer to deformation in which no pore fluid flow occurs. From (2) it is clear that the solid volumetric strain is related to the mean stress σ_{kk} and change in pore fluid mass content through

$$\varepsilon_{kk} = \frac{\sigma_{kk}}{3K_u} + \frac{B\Delta m}{\rho_0} \tag{3}$$

(Appendix A, equation (A5)), where K_u is the undrained bulk modulus.

The solid volumetric strain is seen to be composed of two parts: an undrained elastic strain and a strain resulting from change in pore fluid content. For relatively incompressible fluids, such as oil and water, the latter is very nearly $B\Delta v$, where Δv is the change in pore fluid volume per unit solid volume. In this case, B is therefore the ratio of solid volume change to change in pore fluid volume. The range of B is restricted to $0 \leq B \leq 1$; for water-saturated soils, $B \approx 1$, while for a number of diverse rock types, ranging from sandstones to granites, B ranges from 0.5 to 0.9 [*Rice and Cleary*, 1976]. Thus, for example, if water is uniformly withdrawn from a rock with B of 0.8 the volumetric contraction of the rock is 80% of the volume of extracted water.

Returning to Figure 5a, it is now apparent that the stress-free transformation strain resulting from a uniform change in fluid mass content Δm is simply

$$\varepsilon_{kk}{}^T = B\Delta m/\rho_0 \tag{4}$$

To restore the element to its initial shape, it is necessary to strain elastically the element by $-\varepsilon_{kk}{}^T$, while maintaining the pore fluid mass constant (3 in Figure 5a). The elastic straining is achieved by adding tractions T_i to the surface of the element:

$$T_i = -K_u\varepsilon_{kk}{}^T n_i \tag{5}$$

where n_i is the unit surface normal.

The element (inclusion) at this stage has no net strain and therefore fits precisely into the cut in the half-space (matrix). Once the inclusion is reinserted into the matrix, the surface tractions can be relaxed, allowing the inclusion to contract and strain the matrix. Recall that at present, we are considering only the instantaneous stress changes before pore fluid flow occurs. If the dimensions of the element are small in comparison to the depth of burial, the stresses due to contraction can be adequately represented by a point center of contraction, or negative center of dilatation (Figure 5b). The stresses resulting from the change in fluid mass Δm can be represented by a vertical point force with magnitude Δmg, where g is the acceleration of gravity (Figure 5b).

One can easily show that the stress change due to contraction of the solid dominates the gravitational stress change due to depletion of fluid mass. In the following analysis it proves to be convenient to restrict attention to plane strain deformations ($u_3 = 0$) and to take the inclusion to be a cylinder of radius r_0 with axis parallel to the x_3 direction. Following the steps indicated in Figure 5a, the stresses in the matrix are found to be

$$\sigma_{rr} = -\sigma_{\theta\theta} = \frac{-B(1+\nu_u)\mu\Delta m V^I}{3\pi\rho_0(1-\nu_u)r^2} \tag{6}$$

(equation (B15)), where V^I is the inclusion volume per unit length in the z direction. Equation (6) is valid when the distance from the inclusion r is small in comparison to the burial depth. The effect of a nearby free surface is added in the following section. Note that as expected, extraction of fluid ($\Delta m < 0$) produces radial tension near the inclusion; the circumferential stress is equal in magnitude and opposite in sign.

In Cartesian coordinates the change in stress due to contraction $\sigma_{mn}{}^{\text{contr}}$ ($m, n = 1, 2$) can be written

$$\sigma_{mn}{}^{\text{contr}} = \frac{(1+\nu_u)Bf_{mn}(\theta)}{3\pi\rho_0(1-\nu_u)}\frac{\mu\Delta m V^I}{r^2} \tag{7}$$

where $f_{mn}(\theta)$ is a function of the angle θ measured from the vertical and is of order unity. As discussed above, the effect of fluid mass change is equivalent to a vertical point force of magnitude $V^I\Delta mg$. The stresses due to a point force $\sigma_{mn}{}^{\text{mass}}$ are [*Love*, 1944, p. 209]

$$\sigma_{mn}{}^{\text{mass}} = \frac{g_{mn}(\theta, \nu_u)}{2\pi(1-\nu_u)}\frac{\Delta mg V^I}{r} \tag{8}$$

Where $g_{mn}(\theta, \nu_u)$ is again of order one. The ratio of stress change due to contraction to that due to mass depletion is therefore

$$\frac{\sigma_{mn}{}^{\text{contr}}}{\sigma_{mn}{}^{\text{mass}}} \cong \frac{2B}{3}\frac{\mu}{\rho_0 gr} \tag{9}$$

For reasonable choices of parameters (i.e., $B = 0.6$ [*Rice and Cleary*, 1976], $\mu = 10^4$ MPa, $\rho_0 = 10^3$ kg/m^3, and $g = 10$ m/s^2) the ratio $\sigma_{mn}{}^{\text{contr}}/\sigma_{mn}{}^{\text{mass}}$ is approximately 1000 at $r = 1$ km and 100 at $r = 10$ km. This means that for distances from the producing zones of 10 km or less, the stresses due to contraction are at least two orders of magnitude greater than the stresses due to mass depletion. The change in mass within the producing rocks can therefore be neglected.

Distributed Depletion of Pore Fluid

The general flow equation governing alterations in pore fluid mass is the diffusion equation, i.e.,

$$c\nabla^2(\Delta m) = \partial(\Delta m)/\partial t \tag{10}$$

where the hydraulic diffusivity c of the medium is given by

$$c = \frac{k}{\eta}\left[\frac{2\mu(1-\nu)}{(1-2\nu)}\right]\left[\frac{B^2(1+\nu_u)^2(1-2\nu)}{9(1-\nu_u)(\nu_u-\nu)}\right] \tag{11}$$

where k is permeability (with units of area) and η is the fluid viscosity [*Rice and Cleary*, 1976]. In the limit that the rock behaves as a rigid matrix, equation (11) reduces to

$$c = k/\eta\phi\beta \tag{12}$$

where ϕ is the porosity and β is the fluid compressibility [*Rice and Cleary*, 1976].

Changes of pore fluid content in space and time $\Delta m(x, y, t)$ can be found from (10) as long as the boundary and initial conditions can be posed in terms of pore fluid content or pore fluid flux. In the previous section it was shown that the undrained stresses and displacements due to an isolated change in pore fluid content are proportional to Δm. For the general problem of fluid extraction from a half plane the relation is

$$u_n(x, y, t) = \frac{(1+\nu_u)B\,dV}{3\pi\rho_0(1-\nu_u)}\,\Delta m(\zeta, \xi, t)g_n(x, y; \zeta, \xi) \tag{13}$$

(Appendix C, equation (C13)), where $g_n(x, y; \zeta, \xi)$ is the displacement in the n direction at (x, y) due to a point center of dilatation at (ζ, ξ), and $\Delta m dV$ is the change in fluid mass content at the point (ζ, ξ). It should be clear then that the total displacement due to a distributed change in fluid mass content at time t is obtained by integrating the undrained, point fluid mass changes over the volume for which Δm is nonzero, i.e.,

$$u_n(x, y, t) = \frac{(1+\nu_u)B}{3\pi\rho_0(1-\nu_u)}\int_V \Delta m(\zeta, \xi, t)g_n(x, y; \zeta, \xi)\,dV_\zeta \tag{14}$$

where the subscript on the differential dV_ζ indicates that the integration is with respect to ζ and ξ (not x and y).

The stresses are related to the displacements through the constitutive equations, which making use of the strain-displacement relations (A9), can be written as

$$\sigma_{nm} = \mu\left(\frac{\partial u_n}{\partial x_m} + \frac{\partial u_m}{\partial x_n} + \frac{2\nu_u}{1-2\nu_u}\frac{\partial u_k}{\partial x_k}\delta_{nm}\right) - \frac{BK_u\Delta m}{\rho_0}\delta_{nm} \tag{15}$$

(Appendix A, equation (A10)). Substituting (14) into (15),

$$\sigma_{nm}(x, y, t) = \frac{\mu(1+\nu_u)B}{3\pi\rho_0(1-\nu_u)}\int_V \Delta m(\zeta, \xi, t)G_{nm}(x, y; \zeta, \xi)\,dV_\zeta - \frac{BK_u}{\rho_0}\Delta m(x, y, t)\delta_{nm} \tag{16}$$

where

$$G_{nm} = \frac{\partial g_n}{\partial x_m} + \frac{\partial g_m}{\partial x_n} + \frac{2\nu_u}{1-2\nu_u}\frac{\partial g_k}{\partial x_k}\delta_{nm} \tag{17}$$

The functions G_{nm} relate the stress at (x, y) to a unit center of dilatation at (ζ, ξ) in an undrained medium and are given in Appendix C equation (C11).

Finally, the pore pressure is calculated from the change in pore fluid mass and mean stress through the additional constitutive relation

$$p(x, y, t) = \frac{(1+\nu_u)B}{3}\left[\frac{2(1+\nu_u)\mu B}{3\rho_0(\nu_u-\nu)}\Delta m(x, y, t) - \sigma_{nn}(x, y, t)\right] \tag{18}$$

(equation (A13)), where ν is Poisson's ratio under drained conditions. Substituting the mean stress, from (16) into (18),

$$p(x, y, t) = \frac{2\mu(1+\nu_u)^2B^2}{9\rho_0}\left\{\frac{(1-2\nu)}{(\nu_u-\nu)(1-2\nu_u)}\Delta m(x, y, t) - \frac{1}{2\pi(1-\nu_u)}\int_V \Delta m(\zeta, \xi, t)G_{nn}(x, y; \zeta, \xi)\,dV_\zeta\right\} \tag{19}$$

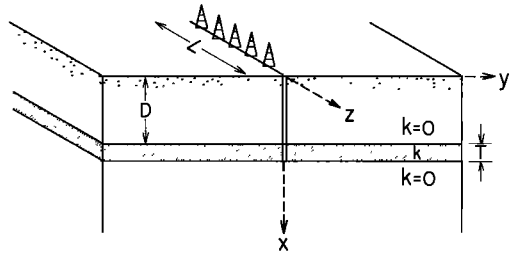

Fig. 6. Layer of thickness T and permeability k buried at a depth D in a fluid-infiltrated, impermeable ($k = 0$) half-space.

In summary, the procedure is to first calculate the change in pore fluid content from the diffusion equation (equation (10)). The induced displacements, stresses, and pore pressure are then calculated from (14), (16), and (19). The Green's functions g_n and G_{nm} for plane strain deformation in an elastically homogeneous half-space are given in Appendix C.

Fluid Extraction From a Horizontal Layer

In this section, stress and deformation changes resulting from the withdrawal of fluid from a permeable layer embedded in a fluid-infiltrated, impermeable half-space are calculated (Figure 6). The thickness T of the layer is taken to be much smaller than the layer depth D. This is a reasonable approximation for the oil fields on Anticline Ridge where T/D for the principal producing horizons is of the order of 0.1. The producing layer has permeability k, while the surrounding rocks are assumed to have negligible permeability. As discussed previously, the oil-bearing horizons are stratigraphically bounded by shales, which are likely to be five orders of magnitude less permeable than the producing sandstones [*Brace*, 1980]. Over the 80-year period of oil production the shales are therefore effectively impermeable.

The oil fields are elongate in a NW-SE direction along the axis of the Coalinga anticline. This geometry is idealized as a line of wells extending indefinitely in the z direction (Figure 6). The fluid flux out of the layer is taken to be independent of position along the z direction. As fluid is withdrawn from the line of wells, flow is induced in the layer toward the plane $y = 0$. Because the surrounding medium is effectively impermeable, flow occurs only in the y direction. Finally, note that the model geometry is such that the induced deformation is one of plane strain; that is, there are no displacements in the z direction.

The flow equation (equation (10)) for one-dimensional flow takes the form

$$c\frac{\partial^2\Delta m}{\partial y^2} = \frac{\partial\Delta m}{\partial t} \tag{20}$$

The net mass flux out of the producing zone $-Q$ is taken to be constant for $t > 0$ and zero for $t < 0$ (the dashed lines in Figure 5). If q is the local fluid mass flux, then the boundary conditions for flow in an inifinite layer are

$$q(y = 0^+) - q(y = 0^-) = -Q \qquad t > 0 \tag{21a}$$

$$q(y = \pm\infty) = 0 \qquad t > 0 \tag{21b}$$

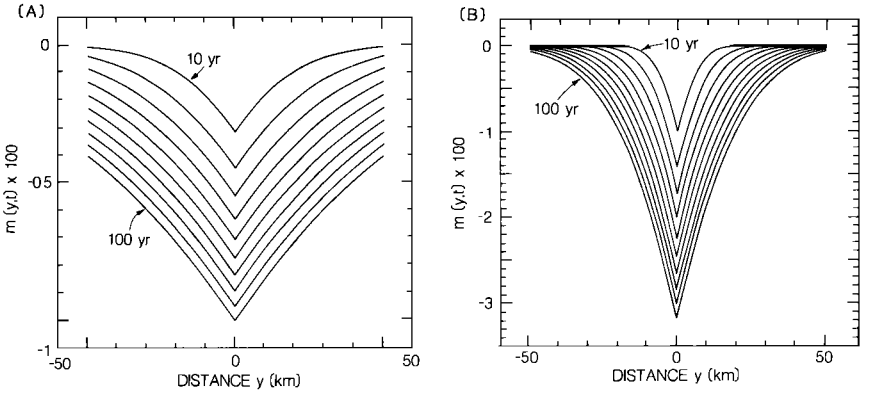

Fig. 7. Change in pore fluid content as a function of position along the permeable layer, calculated from equation (24). Results are for $\dot{V} = 2 \times 10^6$ m^3/yr, $L = 10$ km, $T = 100$ m, $\phi = 0.2$; (*a*) $c = 1.0$ m^2/s and (b) $c = 0.1$ m^2/s.

The solution of (20) subject to boundary conditions (21) is [*Carslaw and Jaeger*, 1959, p. 75]

$$\Delta m(y, t) = -Q(t/c)^{1/2} \text{ ierfc } (y^2/4ct)^{1/2} \qquad t > 0 \qquad (22)$$

where ierfc (x) is the first integral of the complementary error function

$$\text{ierfc } (x) = \int_0^x \text{erfc } (\xi)\, d\xi = \frac{e^{-x^2}}{(\pi)^{1/2}} - x \text{ erfc } (x) \qquad (23)$$

Equation (22) can be put in a somewhat more interpretable form by dividing both sides by the reference fluid density ρ_0. Recalling that Δm is defined as the fluid mass change per unit solid volume, the left-hand side becomes $\mathcal{M}\phi$, where $\mathcal{M}$ is the fractional change in fluid mass and ϕ is the porosity. Thus

$$\mathcal{M}(y, t) = \frac{-\dot{V}}{LT\phi}\left(\frac{t}{c}\right)^{1/2} \text{ierfc}\left(\frac{y^2}{4ct}\right) \qquad (24)$$

where the volume flux Q/ρ_0 has been replaced by $\dot{V}/LT$. Here $\dot{V}/L$ is the average rate of fluid extraction per unit length in the z direction and T is the layer thickness.

The fractional decrease in pore fluid mass $\mathcal{M}$ is shown in Figure 7 for $\dot{V} = 2 \times 10^6$ m^3/yr, $L = 10$ km, $T = 100$ m, $\phi = 0.2$, and $c = 1.0$ m^2/s (Figure 7*a*) and 0.1 m^2/s (Figure 7*b*). As expected, for relatively large diffusivities the fluid depletion is dispersed and the maximum reduction in pore fluid mass is small, whereas for relatively low diffusivities the depletion is concentrated near the point of extraction and the maximum reduction in pore fluid mass is relatively greater.

The vertical displacement of the free surface ($z = 0$) is found from equation (14), where $g_x(x = 0, y; \zeta, \xi)$ is given in Appendix C (equation (C9))

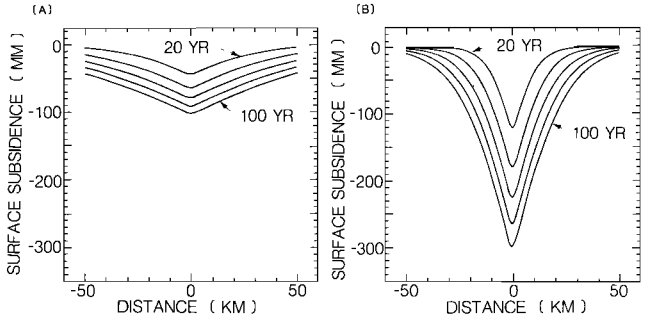

Fig. 8. Free surface subsidence as a function of distance along the surface at five different elapsed times. The producing layer is buried at a depth D of 1 km; $\dot{V} = 2 \times 10^6$ m^2/yr, $L = 10$ km, $B = 0.6$; (*a*) $c = 1.0$ m^2/s and (*b*) $c = 0.1$ m^2/s.

$$u_x(x = 0, y, t) = \frac{-2B(1 + \nu_u)}{3\pi\rho_0} \cdot \int_V \frac{\zeta}{\zeta^2 + (y - \xi)^2} \Delta m(\zeta, \xi, t)\, dV \qquad (25)$$

Note that in this particular problem, Δm is nonzero only within the layer. If, as previously assumed, the layer thickness T is small in comparison to its depth D and Δm is independent of depth within the layer, then making use of (22), equation (25) is approximated by

$$u_x(x = 0, y, t) = \frac{2B(1 + \nu_u)\dot{V}D}{3\pi L}\left(\frac{t}{c}\right)^{1/2} \cdot \int_{-\infty}^{\infty} \frac{\text{ierfc } (\xi^2/4ct)^{1/2}}{D^2 + (y - \xi)^2}\, d\xi \qquad (26)$$

The free surface subsidence above a single producing layer located at a depth of 1 km is shown in Figure 8 for $c = 1.0$ and 0.1 m^2/s. The undrained Poisson's ratio ν_u and Skempton's coefficient B are taken to be 0.33 and 0.6, respectively. The other parameters are the same as in Figure 7.

From (26) it is clear that the subsidence increases linearly with the rate of fluid extraction. The subsidence also depends strongly on hydraulic diffusivity. For high diffusivities the fluid depletion is dispersed, the subsidence is spread over a broad area, and the peak subsidence is relatively small; whereas for low diffusivities the subsidence is localized and the maximum subsidence is relatively large. For $\dot{V} = 2 \times 10^6$ m^3/yr and $c = 1.0$ m^2/s the maximum subsidence rate (at $y = 0$) is approximately 1 mm/yr (Figure 8*a*). For the same rate of withdrawal and $c = 0.1$ m^2/s the maximum subsidence rate is 3 mm/yr (Figure 8*b*).

The stress change due to fluid extraction, given by (16), can be calculated in much the same way as the subsidence. Note first that outside the permeable layer the pore fluid content does not change ($\Delta m = 0$), so that the second term in (16) does not contribute to the stress change outside the layer. An approximation to the stress change is found from (16) which is valid far from the depleted layer, that is, for $|x - D| \gg T$, where again $T/D \ll 1$ and Δm is assumed to be independent of depth within the layer. Substituting (22) into (16),

$$\sigma_{mn}(x, y, t) = \frac{-\mu B(1 + \nu_u)\dot{V}}{3\pi(1 - \nu_u)L}\left(\frac{t}{c}\right)^{1/2} \int_{-\infty}^{\infty} G_{mn}(x, y, D, \xi) \cdot \text{ierfc}\left(\frac{\xi^2}{4ct}\right)^{1/2} d\xi \qquad (27)$$

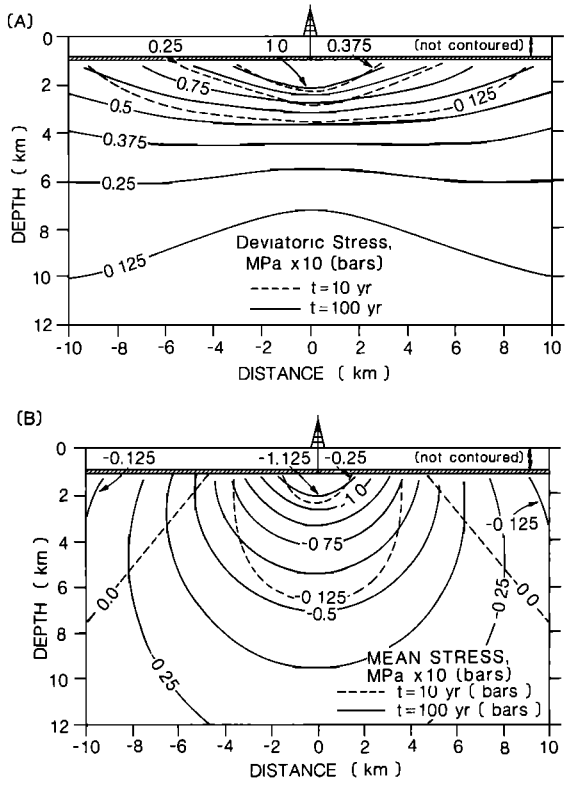

Fig. 9. Stress changes resulting from fluid extraction for a single producing layer of infinite extent. (*a*) Deviatoric stress change $[(\sigma_{xx} - \sigma_{yy})^2/4 - \sigma_{xy}{}^2]^{1/2}$. (*b*) Mean stress change $(\sigma_{xx} + \sigma_{yy})/2$. Contours are lines of equal stress change after 10 years (dashed) and 100 years (solid) of extraction. Negative values of mean stress indicate compression. Results are for $\mu = 5.6 \times 10^3$ MPa and $c = 0.03$ m^2/s. The other parameters are the same as in Figure 8.

Results are illustrated in Figure 9 for a shear modulus μ of 5.6×10^9 Pa, $c = 0.03$ m^2/s, and the same geometry, extraction rate, and material properties as in Figure 8. Although these values are all reasonable, this example is intended only to illustrate the general effects of fluid extraction. It is not intended to reproduce the detailed situation in the Coalinga region; such a calculation is attempted, however, in the following section. Contours of equal deviatoric stress $[(\sigma_{xx} - \sigma_{yy})^2/4 - \sigma_{xy}{}^2]^{1/2}$ (Figure 9*a*) and mean stress $(\sigma_{xx} + \sigma_{yy})/2$ (Figure 9*b*) are shown throughout a region 20 km wide by 12 km deep. The stresses at a given point below the producing horizon change with time. In Figure 9 the dashed contours indicate stress change after 10 years of fluid extraction, while the solid lines indicate stress change after 100 years. For example, there is a 0.0125-MPa (0.125 bar) change in deviatoric stress at 2–3 km depth after 10 years of withdrawal and a 0.05-MPa (0.5 bar) change at comparable depths after 100 years. In general, induced deviatoric stresses decrease with depth below the producing zone. For the parameters used in this calculation the stress changes at 10 km depth are of the order of 0.01 MPa (0.1 bar) for elapsed time less than or equal to 100 years.

The mean stress changes due to fluid extraction also vary with the elapsed time following the onset of extraction. Below the point of extraction ($y = 0$) the mean stress is compressive (negative), while there is slight tension on the flanks. This can be seen in Figure 9*b* for $t = 10$ years (dashed contours). With increasing elapsed time the zone of tension migrates out of the contoured area, so that after 100 years of extraction the entire region illustrated in Figure 9*b* is in compression.

It is worth emphasizing at this point that the stress changes in this example are generated entirely by contraction of the shallow, producing horizon. Fluid flow is completely confined to the producing layer. As discussed previously, shales below the producing layer are effectively impermeable (recall Figure 6) so that there is no fluid transport from depth to the producing zone. In this model the stresses are transmitted to depth elastically, through the solid rock matrix, without direct fluid transport.

As a final point the decrease in pore pressure within the producing zone due to fluid extraction is computed. The pore pressure decline is found from (19), making use of (C11) for the Green's function for mean stress G_{nn} and (22) for Δm. Recalling that Δm is nonzero only for $D \le \zeta \le D + T$, it is possible to solve the integral with respect to ζ exactly to yield

$$p(x, y, t) = \frac{-2\mu(1 + \nu_u)^2 B^2 \dot{V}}{9LT} \left(\frac{t}{c}\right)^{1/2} \cdot \left\{ \frac{(1 - 2\nu)}{(\nu_u - \nu)(1 - 2\nu_u)} \operatorname{ierfc}\left(\frac{y^2}{4ct}\right)^{1/2} - \frac{2}{\pi(1 - \nu_u)} \cdot \int_{-\infty}^{\infty} \left[\frac{(x + D)}{(x + D)^2 + (y - \xi)^2} - \frac{(x + D + T)}{(x + D + T)^2 + (y - \xi)^2} \right] \cdot \operatorname{ierfc}\left(\frac{\xi^2}{4ct}\right)^{1/2} d\xi \right\} \quad (28)$$

Application of Method to the Coalinga Area

For the purposes of this study there are three principal oil-producing zones: Coalinga Westside, Coalinga Eastside, and the nose region of the Coalinga East Extension. The geometry adopted to model the effects of fluid extraction in this area is illustrated in Figure 10. The Temblor Formation, which extends between the East and West Coalinga fields, is located at a depth of 0.6 km, the average depth of the Temblor in the Coalinga Eastside field [*California Division of Oil and Gas*, 1973]. In the calculation 1.6×10^6 m^3/yr of liquid is extracted from the Eastside beginning in 1905 (refer to Figure 3*a*). The rate of extraction from the Westside is 1.1×10^6 m^3/yr, also beginning in 1905. The Gatchell sand, which grades into the so-called Turritella silt southwest of Anticline Ridge, is modeled as a semi-infinite layer located at a depth of 2.3 km. 3.7×10^6 m^3/yr of liquid was extracted from the Gatchell beginning in 1940 (refer to Figure 3*b*).

The material properties used in the calculation are summarized in Table 1. Thickness T, porosity ϕ, and permeability k for both the Gatchell and Temblor are given by *California Division of Oil and Gas* [1973]. Measured permeabilities of Temblor range from 3×10^{-13} m^2 (300 mdarcy) to 10^{-11} m^2 (10,000 mdarcy); however, 2×10^{-12} m^2 (2000 mdarcy) is considered to be representative of the entire horizon (R. Curtain, personal communication, 1983). Oil viscosities are also variable. Oil produced from the Gatchell has a viscosity of approximately 10^{-3} Pa s (1 cP). Viscosities of Temblor oils, however, range from 10^{-2} Pa s (10 cP) to 2.5 Pa s (2500 cP) [*California Division of Oil and Gas*, 1973], with an average over the life of the field of 0.15–0.2 Pa s (150–200 cP) (R. Curtain, personal communication, 1983). Considering that nearly half of the net liquid withdrawn from the Temblor is water (Figure 3*a*), 0.1 Pa s (100 cP) is taken to be a reasonable value for the average liquid viscosity. Using the above values,

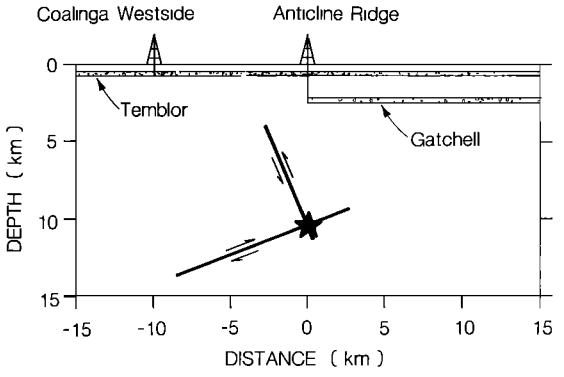

Fig. 10. Geometry used to model stress change and subsidence in the Coalinga region.

hydraulic diffusivities calculated from equation (12) are 0.2 m^2/s for the Temblor and 7.0 m^2/s for the Gatchell (Table 1). The uncertainty in permeability and viscosity appropriate for the Temblor zone lead to uncertainties in the calculated diffusivity for the Temblor. It is possible that the actual diffusivity may be as low as 0.02 m^2/s.

Skempton's coefficient and Poisson's ratio under undrained conditions are not routinely measured and are not available for either the Gatchell or Temblor. The values used in the calculations here (Table 1) are those given by *Rice and Cleary* [1976] for the Berea Sandstone. The shear moduli of the producing rocks have not been reported but can be inferred from borehole velocity measurements. Compressional wave velocities in the Gatchell sand average 3.8 km/s, corresponding to shear moduli of 8×10^3 to 12×10^3 MPa assuming a density of 2300 kg/m^3 and Poisson's ratio between 0.2 and 0.33.

The change in stress acting on the two nodal planes due to liquid extraction was calculated using the methods developed in the previous section. The material parameters used in the calculation are listed in Table 1. The location and dip of the two model fault planes were chosen to be consistent with the main shock location and focal mechanism. For the northeast dipping plane the top of the slipped zone is at a depth of 4.0 km, the base at 11.2 km [*Stein*, 1983]. For the southwest dipping plane the top of the slipped surface is at a depth of 9.5 km and the base at 13.5 km (Figure 10). The stresses were rotated into the possible fault planes to determine the shear and normal stress acting across these surfaces. These stresses represent the changes in the existing stress state due to extraction of liquid from the Temblor formation and Gatchell sand. The total stress is the sum of the existing tectonic stress and the stress resulting from extraction.

TABLE 1. Average Properties of Producing Horizons

	Temblor	Gatchell
Depth D, km	0.6	2.3
Thickness T, m	75	0–190
Rate of liquid extraction $-\dot{V}$, m^3/yr	1.6×10^6	3.7×10^6
Extraction starts, year	1905	1940
Characteristic length along strike, L km	10	10
Porosity ϕ	0.3	0.2
Permeability k, m^2	2×10^{-12}	4.2×10^{-13}
Liquid compressibility β, Pa^{-1}	3×10^{-10}	3×10^{-10}
Viscosity η, Pa s	0.1	10^{-3}
Diffusivity c, m^3/s	0.2	7.0
Skempton's coefficient B	0.6	0.6
Poisson's ratio		
Undrained ν_u	0.33	0.33
Drained ν	0.20	0.20
Shear modulus μ, Pa	8×10^9	8×10^9

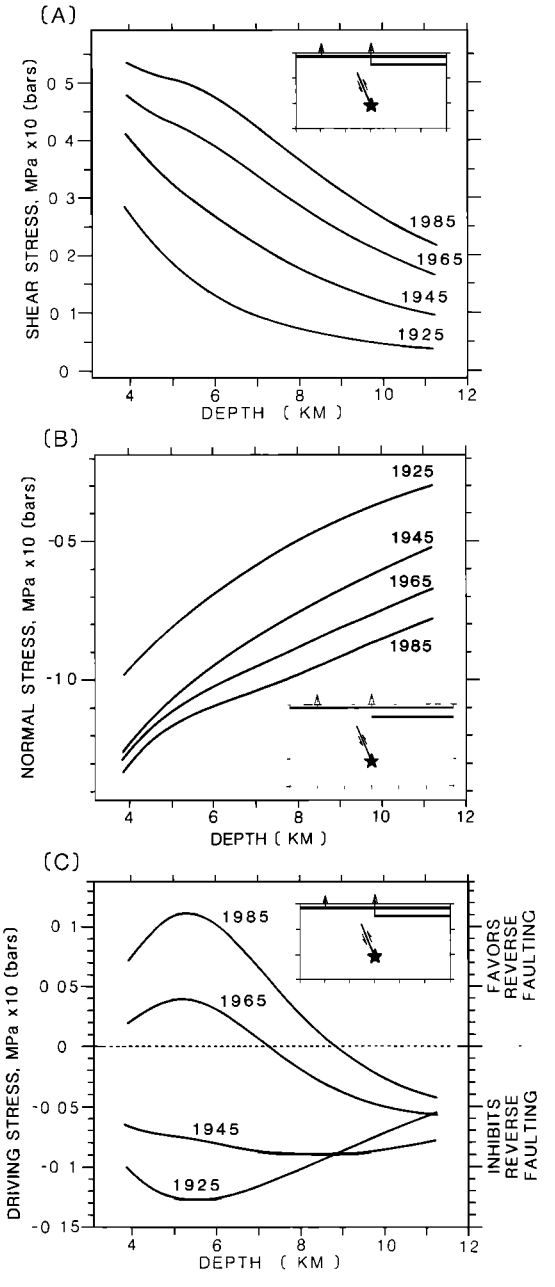

Fig. 11. Change in stresses resolved on the northeast dipping plane due to fluid extraction as a function of depth. Stress changes are shown at four different times. Extraction from the Temblor Formation begins in 1905, from the Gatchell sand in 1940. (*a*) Change in resolved shear stress. Positive shear stresses favor reverse slip on fault. (*b*) Change in resolved normal stress. Negative normal stresses indicate compression, which inhibits frictional slip. (*c*) Change in resolved "driving stress," $\Delta\sigma_s + f(\Delta\sigma_n + \Delta p)$. The coefficient of friction f is taken to be 0.6. The pore pressure change Δp is the undrained or "instantaneous," response to changes in mean stress. Positive values of driving stress favor reverse slip, negative values inhibit slip.

Northeast Dipping Plane

The change in resolved shear stress on the 67° northeast dipping plane is shown in Figure 11*a* as a function of depth.

Each curve in Figure 11*a* represents the stress change at a given time following the onset of extraction. The sign convention employed is such that positive shear stresses favor reverse faulting. Note that the shear stresses favor reverse faulting on a high angle fault beneath Anticline Ridge. The magnitudes of the stresses, however, are small: less than 0.04 MPa (0.4 bar) at depths of 8 km or more.

The corresponding changes in normal stress acting across the fault are shown in Figure 11*b*. The normal stresses are found to be compressive (negative) for all depths and times of interest. In general, the magnitude of the induced compression decreases with depth and increases at a given depth with time following the onset of extraction.

The change in driving stress $\Delta\sigma_d$ is calculated in order to assess the net effect of changing shear and normal stresses on the fault. The driving stress $\Delta\sigma_d$ is defined as

$$\Delta\sigma_d = \Delta\sigma_s + f(\Delta\sigma_n + \Delta p) \tag{29}$$

where $\Delta\sigma_s$ and $\Delta\sigma_n$ are the change in shear and normal stress, f is the coefficient of friction, and Δp is the change in pore pressure. Although the calculations involve no fluid transport to or from the fault, there is an undrained, or "instantaneous," pore pressure change due to changes in mean stress σ_{nn}. The undrained pressure response is found by setting $\Delta m = 0$ in equation (13).

$$\Delta p = -\frac{(1+\nu_u)B}{3}\Delta\sigma_{nn} \qquad n = 1, 2 \tag{30}$$

Substituting (30) into (29) yields an expression for the driving stress in the form

$$\Delta\sigma_d = \Delta\sigma_s + f\left[\Delta\sigma_n - \frac{(1+\nu_u)B}{3}\Delta\sigma_{nn}\right] \tag{31}$$

The change in driving stress acting on the northeast dipping plane is shown in Figure 11*c*, assuming a coefficient of friction of 0.6. Near the hypocenter, that is, for depths greater than 9 km, the increased compression dominates the increased shear stress. The situation reverses at shallow depths after approximately 50 years of extraction. There the increased shear stresses dominate causing an increase in the driving stress. The net effect of fluid extraction is to inhibit slightly the slip on the northeast dipping plane in the vicinity of the hypocenter and to favor slightly the slip on the same plane at shallow depths.

Southwest Dipping Plane

The change in shear stress acting on the southwest dipping plane as a function of depth is shown in Figure 12*a*. The sign convention is such that positive shear stresses favor reverse faulting. As in the case for the northeast dipping plane, the shear stresses generated by extraction favor reverse faulting on a deep, low-angle fault beneath Anticline Ridge. The maximum shear stress in this case is slightly less than 0.03 MPa (0.3 bar). The induced normal stresses acting across the southwest dipping plane (Figure 12*b*) are compressive, tending to inhibit slip.

The change in driving stress acting across the southwest dipping plane is shown in Figure 12*c*. In contrast to the result for the steeply dipping plane, the change in driving stress is of the correct sense to favor reverse motion on the southwest dipping plane. At the time of the earthquake the driving stress increased by nearly 0.02 MPa (0.2 bar) at a depth of 9.5 km and 0.01 MPa (0.1 bar) at 13.5 km.

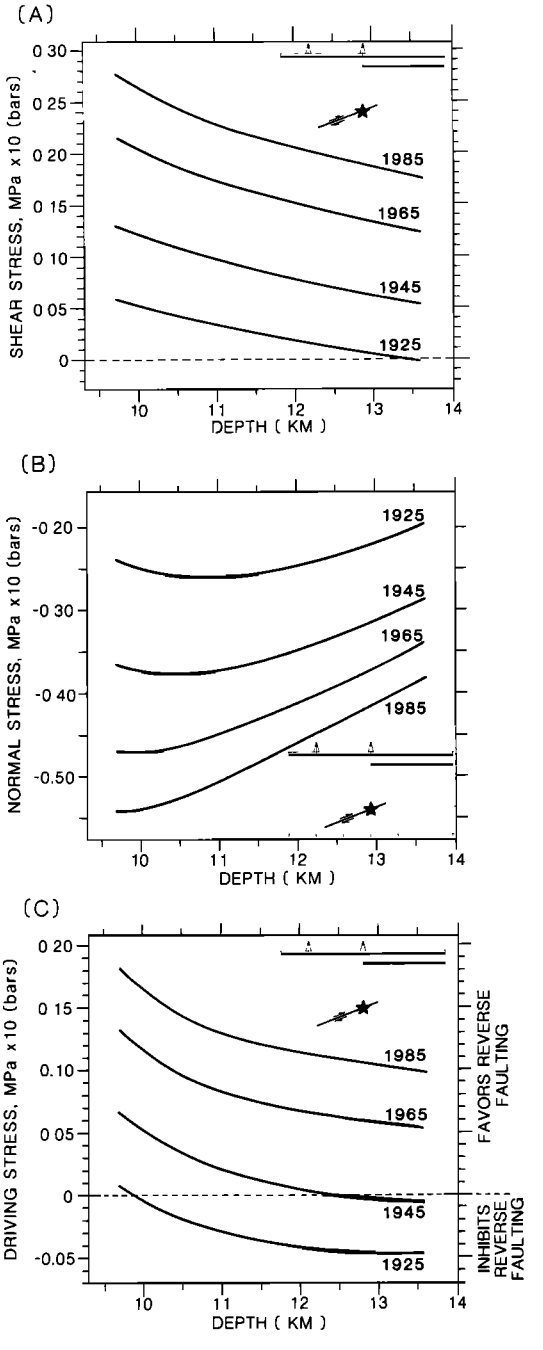

Fig. 12. Change in stresses resolved on the southwest dipping plane. (*a*) Shear stress. (*b*) Normal stress. (*c*) Driving stress. Sign convention is the same as in Figure 11.

Subsidence

As an independent check on the analytical methods employed to calculate stress change, the theory can be used to calculate the subsidence of Anticline Ridge resulting from fluid extraction. The calculated subsidence can then be compared with observed elevation changes of benchmarks on Anticline Ridge determined by repeated leveling surveys. The parameters used in this calculation are the same as those employed in the previous stress calculation (Table 1). Three benchmarks on Anticline Ridge (W156, V156, and V237) were chosen for this comparison because they are located on Tertiary rocks and should not be influenced by soil subsidence related to ground-

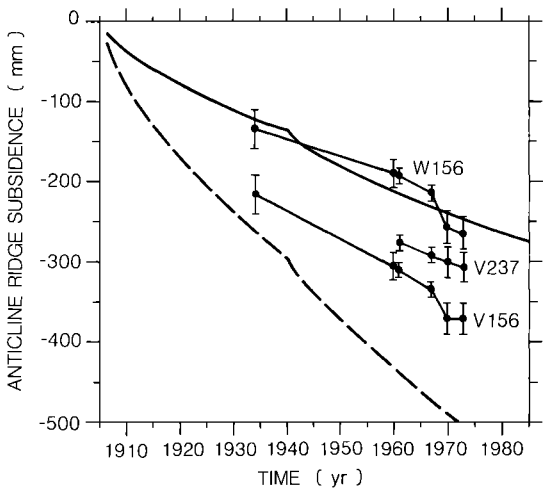

Fig. 13. Observed elevation changes of three bench marks (W156, V156, and V237) on Anticline Ridge, compared with vertical displacements calculated from equation (26). Solid curve illustrates subsidence calculated with the hydraulic diffusivity of the Temblor Formation equal to the preferred value of 0.2 m^2/s. Dashed curve illustrates the effect of decreasing this value to 0.02 m^2/s. The diffusivity of the Gatchell sand is 7.0 m^2/s in both cases. Error bars indicate estimated uncertainties in the leveling data, including both random errors and possible refraction errors in the 1933–1935 and 1958–1959 surveys (see discussion in text).

water pumping. All three benchmarks were surveyed in 1960, 1966, 1969, and 1972 [*Stein*, 1983] (National Geodetic Survey lines L17723, L20605, L21703, L22671). In addition, benchmarks W156 and V156 were surveyed in 1933–1935 and 1958–1959 [*Prokopovich and Magleby*, 1968]. The 1958–1959, 1960, and 1966 surveys were performed to first-order standards; the 1933–1935, 1969, and 1972 surveys to second-order standards.

Elevation changes of the Anticline Ridge benchmarks relative to an assumed stable site on Cretaceous rocks within the Diablo Range west of Coalinga (benchmarks F1046 [*Stein*, 1983] and F156 [*Prokopovich and Magleby*, 1968]) are shown in Figure 13. The 1960 to 1972 leveling has been corrected for refraction error [*Stein*, 1983] by using the method of *Holdahl* [1981]. The 1933–1935 and 1958–1959 data are not corrected for refraction error; however, the reference station is nearly at the same elevation as Anticline Ridge, so that these errors should be less than 15 mm. In fact, the refraction corrections for W156 and V156 between 1960 and 1966 are only 5 and 7 mm, respectively. Random errors between the reference station and Anticline Ridge are assumed to be less than 9 mm for first-order leveling and 19 mm for second-order leveling.

The average subsidence rate of benchmarks W156 and V156 between 1933 and 1972 were 3.2 ± 0.6 and 4.1 ± 0.4 mm/yr, respectively (Figure 13). Benchmark V237 subsided at a rate of 2.6 ± 0.1 mm/yr between 1960 and 1972. The mean subsidence rate of Anticline Ridge from these data is 3.3 ± 0.7 mm/yr. The model subsidence calculated by setting $y = 0$ in equation (26) is also shown in Figure 13. The calculated subsidence is in good agreement with the observed elevation changes. In fact, the subsidence rate between 1933 and 1972 predicted by the model is 3.3 mm/yr. It is worth emphasizing that the model parameters are all independently determined; none of the parameters was adjusted to fit the measured elevation changes. Never the less, the material parameters, including hydraulic diffusivity, are imperfectly known. For comparison, the effect of decreasing the diffusivity of the Temblor by one order of magnitude to 0.02 m/s is shown in Figure 13. The average subsidence rate for the same time interval in this case is 6.6 mm/yr, roughly twice the observed rate.

Reservoir Pressure

As a further check, the predicted pore pressure change is compared to the observed pressure decline in the Gatchell sand. Note from equation (28) that the pore pressure change depends on a number of parameters which do not influence the subsidence, namely, shear modulus μ, drained Poisson's ratio ν, and layer thickness T. The pressure change is in fact sensitive to the difference between the undrained and drained Poisson's ratio. In the calculation presented here, ν is taken to be 0.2, so that $\nu_u - \nu = 0.13$. Of the three standstones considered by *Rice and Cleary* [1976] this difference ranged from 0.13 to 0.19. The pressure change in the Gatchell also depends inversely on the layer thickness, which ranges from 0 to 190 m.

The predicted pore pressure change, found by evaluating equation (28) at $x = D + T/2$ and $y = 0$, is compared to the observed pressure decline in the Gatchell sand in Figure 4. Results are shown for thicknesses of the Gatchell of 190, 95, and 60 m. For a thickness of 190 m the predicted pressure decline is approximately a factor of 2 less than observed. This discrepancy could be due to a number of causes. Considering the variable thickness of the Gatchell and the possibility of variable properties within the zone, it is likely that the actual thickness of the producing section is somewhat less than 190 m. Decreasing the thickness by a factor of 2 yields a reasonably good fit to the measured pressures. The misfit in calculated pressures might also result from inaccurate estimates of material properties. For example, an equally good fit to the data is obtained by increasing the drained Poisson's ratio from 0.20 to 0.28. Given the simplicity of the model, the overall fit to the data is adequate. Of course, the detailed features of the pressure history are not reproduced. This is, in a large part, due to the fact that the actual fluid extraction rate is not constant as assumed in the calculation (see Figure 3*b*).

DISCUSSION

At the present time, stress changes at seismogenic depths resulting from fluid extraction cannot be measured directly and must therefore be inferred from near-surface observations. At first glance it might appear that stresses inferred in this way would be almost entirely unconstrained. On the other hand, the analytical methods used to compute stress can also be used to calculate other quantities, such as surface displacement or reservoir pressure, which can be measured directly. Quantitative agreement between theory and observation would then lend credence to the stresses calculated at depths which are currently inaccessible to direct measurements.

The excellent agreement between calculated subsidence rate and observed rate of elevation change on Anticline Ridge (Figure 13) is therefore particularly significant. The consistency between the calculated decline in reservoir pressure and measured pressures in the Gatchell lends further support to the calculated stresses. The agreement between theory and observation is particularly encouraging because the parameters in the theory are either known from independent observations or can be inferred from measurements on similar rocks.

Of course, uncertainties in these parameters lead to uncertainties in the calculated stresses. The magnitude of these uncertainties can be estimated from the equations used to calculate stress (i.e., equation (27)). It is more difficult to estimate uncertainties in the calculations that arise from assumptions in the analysis. For example, it has been assumed here that the

pore fluid is a single liquid phase. A more sophisticated analysis might include three pore fluids (oil, water, and gas) all with different densities, compressibilities, and viscosities. It has also been assumed that the producing horizon has the same elastic properties as the surrounding material to which it is perfectly bonded. The assumption of elastic homogeneity is discussed below; the assumption of perfectly bonded interfaces is more difficult to address. One certainly expects different stresses in the underlying region if the producing horizon is free to slip relative to the adjacent strata. Finally, the present analysis approximates the complex material behavior with a simple linearized constitutive law. Nonlinear and irreversible effects are almost certain to occur with large changes in pore fluid content. The significance of these approximations is left for future study. At the present time it is only possible to assess accurately the significance of uncertainties in measured parameters which appear in the analysis of stress and displacement.

Skempton's coefficient B, for example, is not known directly for the rocks in the Coalinga region, yet the total variation in this parameter is small and should not present a significant source of error. Three liquid (oil or water) infiltrated sandstones considered by *Rice and Cleary* [1976] had Skempton's coefficients ranging between 0.6 and 0.9. An increase in B from 0.6 to 0.9 in the calculations would lead to a 50% increase in the model subsidence rates and stresses.

The shear modulus μ of the Gatchell sand was inferred from borehole velocity measurements. Uncertainties in μ arise from the time scale of the measurements (microseconds for sonic velocities in comparison to decades for fluid extraction), and heterogeneity of elastic properties in the crust beneath Anticline Ridge. Elastic constants determined from velocity measurements may be somewhat higher than in situ elastic properties appropriate for longer time scales. The value determined from borehole velocity logs should therefore be considered as an upper bound on μ.

Uncertainties also arise from heterogeneity in elastic properties, particularly with depth. The rigidity at hypocentral depths may be somewhat greater than the rigidity of the producing rocks. The effect of vertical heterogeneity on the calculated stresses at depth can be estimated from the results of *Dundurs and Guell* [1965] for a center of dilatation in a bimaterial. *Dundurs and Guell* [1965] treat the problem of two bonded half-spaces with different elastic properties. A center of dilatation is located in one half-space, with elastic constants μ_1 and ν_1. The ratio of the stress in the adjoining half-space, with constants μ_2 and ν_2, to the stress due to the same center of dilatation in a homogeneous full-space is

$$\frac{\mu_2}{\mu_1}\left[\frac{1+\kappa_1}{1+\kappa_1\mu_2/\mu_1}\right] \tag{32}$$

where

$$\kappa_1 = 3 - 4\nu_1$$

For reasonable values of ν_1 the ratio of stress in the adjoining half-space to stress in a homogeneous region ranges from 1.2 for $\mu_2/\mu_1 = 2$ to 1.5 for $\mu_2/\mu_1 = 10$. Although these results are not strictly appropriate to a layered half-space, they do indicate that the calculated stresses acting at hypocentral depths would be increased by only 50% if the rigidity near the hypocenter is an order of magnitude greater than the rigidity of the producing layers.

Uncertainties in hydraulic diffusivity c arise from the use of equation (12), which assumes flow through a rigid rock matrix, as well as uncertainties in the measurements of permeability and viscosity. *Rice and Cleary* [1976] note that for the Weber Sandstone the value of c computed from the approximate relation (equation (12)) is 60% greater than that computed from the correct expression (equation (11)). This discrepancy is substantially less than the uncertainties in the measurements permeabilities and viscosities, indicating that the use of equation (12) is not a significant source of error.

For a number of reasons the hydraulic diffusivities, particularly of the Temblor, are likely to be accurate only to within an order of magnitude. Decreasing the diffusivity of the Temblor by an order of magnitude was found to increase the predicted subsidence rate from 3 to 6 mm/yr, significantly greater than the observed rate of 3.3 ± 0.7 mm/yr. The change in stress acting on the fault also depends nonlinearly on diffusivity. Stress changes calculated for a range of diffusivities, assuming only that the diffusivities are known to within an order of magnitude, exhibit somewhat varied behavior. In some cases the changes in driving stress are negative, indicating that extraction inhibits slip. In other cases the driving stress changes are positive. For the northeast dipping plane the driving stress changes are always less than 0.04 MPa (0.4 bar) at depth of 8 km or more, and less than 0.075 MPa (0.75 bar) anywhere on the fault surface. The change in driving stress acting on the southwest dipping plane tends to be positive for all plausible combinations of hydraulic diffusivities. The magnitudes of the driving stress changes are less than or equal to 0.03 MPa (0.3 bar) at hypocentral depths on the southwest dipping plane.

It is difficult to evaluate the effect of these relatively small stress changes on the stability of a tectonically loaded fault. One possibility is to compare the stress changes resulting from fluid extraction with the stress drop of the Coalinga earthquake. Using the usual relationship for stress drop [*Chinnery*, 1969] and taking the average slip and fault width to be 1.8 m and 8 km, respectively [*Stein*, 1983], the average stress drop of the main shock is found to be of the order of 10 MPa (100 bars), the precise value depending on assumptions about the geometry of the fault plane. The change in driving stress due to fluid extraction at hypocentral depths (10 ± 1 km) is thus less than 0.2% of the stress drop. For the range of diffusivities considered plausible here, the change in driving stress at hypocentral depths is no greater than 0.4% of the stress drop.

A second, and perhaps more interesting, comparison is to contrast extraction-induced stresses with stresses resulting from the solid earth tides. Tidal stresses within the crust have amplitudes of the order of 5×10^{-3} MPa [*Stacey*, 1969]. The shear stresses induced by fluid extraction are 3 to 4×10^{-2} MPa, an order of magnitude greater than the tidal stresses. Thus, although extraction-induced stresses ar small, they can not be ruled out as a potential triggering mechanism solely because of their small magnitude.

If the rate of tectonic stress accumulation across the Coalinga fault were known, it would be possible to compare the natural stress rate with the stresses induced by extraction. To take a purely hypothetical example, if the average rate of tectonic stress accumulation is 0.1 bar/yr and the main shock fault surface is the southwest dipping plane, then the effect of fluid extraction might have been to shorten the interearthquake time by 1–2 years. Similarly, if the average tectonic stress rate is 0.01 bar/yr, then extraction would be expected to advance the time of the earthquake by one to two decades. If, on the other hand, the steeply, northeast dipping plane is the

main shock surface, then the most likely effect of extraction would have been to increase the interearthquake time by a comparable amount. These examples clearly demonstrate that in order to assess properly the significance of the stress changes calculated here, it will be necessary to determine the tectonic rate of stress accumulation (or the recurrence interval) and to identify which of the two possible planes was the main shock fault plane.

CONCLUSIONS

The presence of thick argillaceous units below the oil-producing horizons is almost certain to have prevented flow of pore fluids between the oil fields and the focal region of the 1983 Coalinga earthquake. In any case, the dominant effect of oil field operations (namely, extraction of pore fluids) has been to decrease pore pressures in the producing strata. In the unlikely event that fluid transport occurred between the producing zones and the earthquake focus, the result would have been to diminish pore pressures along the fault zone, thereby inhibiting frictional slip.

Extraction of large volumes of fluid from the oil fields resulted in a 50% decrease in pore pressure within the Gatchell sand between 1938 and 1983 and caused Anticline Ridge to subside at approximately 3 mm/yr. Stress changes at hypocentral depths, calculated from a model based on Biot's constitutive theory for fluid-infiltrated elastic media, are small in comparison to the earthquake stress drop. The calculated driving stress (shear stress minus frictional resistance) depends on the hydraulic diffusivity of the producing rocks and the orientation of the fault plane. For the steeply northeast dipping plane the driving stress increased by less than 0.01 MPa (0.1 bar) at depths of 4–9 km, weakly favoring slip at shallow depths. At depths of 9–11 km, fluid extraction decreased the driving stress by less than 0.005 MPa (0.05 bar), slightly inhibiting slip near the earthquake hypocenter. For the shallow, southwest dipping plane the driving stress increased by less than 0.02 MPa (0.2 bar), slightly favoring fault slip. Although the calculated stress changes are not easily verified by direct measurement, the ability of the theory to explain quantitatively the observed changes in the elevation of Anticline Ridge and reservoir pressures in the Gatchell sand suggest that the method yields reasonable estimates of stress change at depth.

APPENDIX A: CONSTITUTIVE EQUATIONS FOR POROELASTIC MEDIA

Rice and Cleary [1976], following *Biot* [1941], write the constitutive equations for linear, isotropic, fluid-infiltrated, porous media in the following form:

$$2\mu\varepsilon_{ij} = \sigma_{ij} - \frac{\nu}{1+\nu}\sigma_{kk}\delta_{ij} + \frac{3(\nu_u - \nu)}{B(1+\nu)(1+\nu_u)}p\,\delta_{ij} \tag{A1}$$

$$\Delta m = m - m_0 = \frac{3\rho_0(\nu_u - \nu)}{2\mu B(1+\nu)(1+\nu_u)}\left[\sigma_{kk} + \frac{3}{B}p\right] \tag{A2}$$

Here, ε_{ij} and σ_{ij} are the solid strains and stresses, p is the pore pressure, and m is the mass of pore fluid per unit solid volume; m_0 and ρ_0 are the pore fluid mass and density in the reference state. The constitutive relations contain four constants: μ, ν, ν_u, and B; μ and ν are ordinary ("drained") shear modulus and Poisson's ratio of the solid; ν_u is the Poisson's ratio under "undrained" ($\Delta m = 0$) conditions. "Skempton's pore pressure coefficient" B relates the induced pore pressure to the mean stress under undrained conditions. This is clearly seen by setting $\Delta m = 0$ in (A2).

Equation (A2) can be used to eliminate p from (A1). This gives

$$2\mu\varepsilon_{ij} = \sigma_{ij} - \frac{\nu_u}{1+\nu_u}\sigma_{kk}\delta_{ij} + \frac{2\mu B\,\Delta m}{3\rho_0}\delta_{ij} \tag{A3}$$

and

$$p = \frac{B}{3}\left[\frac{2\mu B\Delta m(1+\nu)(1+\nu_u)}{3\rho_0(\nu_u - \nu)} - \sigma_{kk}\right] \tag{A4}$$

The volumetric strain ε_{kk} is found by setting $i = j$ in (A3) and recalling $\delta_{ii} = 3$:

$$\varepsilon_{kk} = \frac{\sigma_{kk}}{3K_u} + \frac{B\Delta m}{\rho_0} \tag{A5}$$

where the undrained bulk modulus is defined by

$$K_u = \frac{2\mu(1+\nu_u)}{3(1-2\nu_u)} \tag{A6}$$

Equations (A3) can be inverted to give

$$\sigma_{ij} = 2\mu\varepsilon_{ij} + \lambda_u\varepsilon_{kk}\delta_{ij} - \frac{BK_u\Delta m}{\rho_0}\delta_{ij} \tag{A7}$$

where the undrained Lame constant is defined by

$$\lambda_u = \frac{2\nu_u\mu}{1-2\nu_u} \tag{A8}$$

Using the strain displacement equations

$$\varepsilon_{ij} = \frac{1}{2}\left(\frac{\partial u_i}{\partial x_j} + \frac{\partial u_j}{\partial x_i}\right) \tag{A9}$$

equation (A7) can be rewritten as

$$\sigma_{ij} = \mu\left(\frac{\partial u_i}{\partial x_j} + \frac{\partial u_j}{\partial x_i}\right) + \lambda_u\left(\frac{\partial u_k}{\partial x_k}\right)\delta_{ij} - \frac{BK_u\Delta m}{\rho_0}\delta_{ij} \tag{A10}$$

The constraint of plane strain requires $\varepsilon_{13} = \varepsilon_{23} = \varepsilon_{33} = 0$. From (A3), setting $\varepsilon_{33} = 0$

$$\sigma_{33} = \nu_u(\sigma_{11} + \sigma_{22}) - \frac{2(1+\nu_u)\mu B\Delta m}{3\rho_0} \tag{A11}$$

The constitutive relations (A3) and (A4) therefore become

$$2\mu\varepsilon_{mn} = \sigma_{mn} - \nu_u\sigma_{pp}\delta_{mn} + \frac{2(1+\nu_u)\mu B\Delta m}{3\rho_0}\delta_{mn} \tag{A12}$$

and

$$p = \frac{(1+\nu_u)B}{3}\left[\frac{2(1+\nu_u)\mu B\Delta m}{3\rho_0(\nu_u - \nu)} - \sigma_{nn}\right] \tag{A13}$$

where m and n take on the values 1, 2. Setting $m = n$ in (A12), it is evident that

$$\varepsilon_{mm} = \frac{(1-2\nu_u)}{2\mu}\sigma_{mm} + \frac{2(1+\nu_u)B\Delta m}{3\rho_0} \tag{A14}$$

APPENDIX B: STRESS AND DISPLACEMENT RESULTING FROM WITHDRAWAL OF FLUID FROM A CYLINDRICAL INCLUSION

A cylindrical inclusion of radius r_0 is removed from a fluid infiltrated elastic full-space (Figure 5). Fluid is uniformly extracted from the inclusion causing the pore fluid mass to decrease, and the inclusion to undergo a uniform radial strain $\varepsilon_{rr}{}^T$. The inclusion is then stressed, restoring it to its initial

size, and welded back into the matrix. From the general results of *Eshelby* [1957] it is known that the resultant strain in the inclusion is uniform. Choosing a cylindrical coordinate system centered on the inclusion, this result implies that the displacements within the inclusion must be of the form

$$u_r{}^I = A_1 r \qquad u_\theta{}^I = 0 \tag{B1}$$

where A_1 is a constant to be solved for. From elasticity theory it is known that the radial displacements due to a line of centers of dilatation are proportional to r^{-1} [*Love*, 1944], so that the matrix displacements must be of the form

$$u_r{}^M = A_2/r \qquad u_\theta{}^M = 0 \tag{B2}$$

where, again, A_2 is a constant. The strains corresponding to these displacements are

$$\varepsilon_{rr}{}^I = \varepsilon_{\theta\theta}{}^I = A_1 \qquad \varepsilon_{r\theta}{}^I = 0 \tag{B3}$$

and

$$\varepsilon_{rr}{}^M = -\varepsilon_{\theta\theta}{}^M = -A_2/r^2 \qquad \varepsilon_{r\theta}{}^M = 0 \tag{B4}$$

The stresses found by inserting (B3) and (B4) into (A7), noting that $\Delta m = 0$, are

$$\sigma_{rr}{}^I = \sigma_{\theta\theta}{}^I = 2A_1(\mu + \lambda_u) \qquad \sigma_{r\theta}{}^I = 0 \tag{B5}$$

and

$$\sigma_{rr}{}^M = -\sigma_{\theta\theta}{}^M = -2\mu A_2/r^2 \qquad \sigma_{r\theta}{}^M = 0 \tag{B6}$$

The constants A_1 and A_2 are found by requiring that the radial stress is continuous across the boundary of the inclusion $r = r_0$, and the elastic displacements are discontinuous across the boundary by an amount proportional to the (inelastic) transformation strain. The first condition requires that

$$\sigma_{rr}{}^I|_{r=r_0} = \sigma_{rr}{}^M|_{r=r_0} \tag{B7}$$

The second condition requires that

$$u_r{}^M|_{r=r_0} - u_r{}^I|_{r=r_0} = \varepsilon_{rr}{}^T r_0 \tag{B8}$$

(no sum on r). Substituting (B5) and (B6) into (B7) and (B1) and (B2) into (B8) results in a pair of equations in A_1 and A_2 which have the solution

$$A_1 = -\frac{\mu}{\lambda_u + 2\mu}\varepsilon_{rr}{}^T = -\frac{(1-2\nu_u)}{2(1-\nu_u)}\varepsilon_{rr}{}^T \tag{B9}$$

$$A_2 = \frac{\lambda_u + \mu}{\lambda_u + 2\mu}\varepsilon_{rr}{}^T r_0{}^2 = \frac{1}{2(1-\nu_u)}\varepsilon_{rr}{}^T r_0{}^2 \tag{B10}$$

Substituting (B10) into (B2) and (B6) and noting that $\varepsilon_{mm}{}^T = 2\varepsilon_{rr}{}^T$ the matrix displacements and stresses are found to be

$$u_r{}^M = \frac{\varepsilon_{mm}{}^T r_0{}^2}{4(1-\nu_u)r} \tag{B11}$$

and

$$\sigma_{rr}{}^M = -\sigma_{\theta\theta}{}^M = -\frac{\mu}{2(1-\nu_u)}\varepsilon_{mm}{}^T\left(\frac{r_0}{r}\right)^2 \tag{B12}$$

from Appendix A (equation (A14))

$$\varepsilon_{mm}{}^T = \frac{2(1+\nu_u)B\Delta m}{3\rho_0} \tag{B13}$$

so that

$$u_r{}^M = \frac{(1+\nu_u)B\Delta m}{6\pi\rho_0(1-\nu_u)r}V^I \tag{B14}$$

and

$$\sigma_{rr}{}^M = -\sigma_{\theta\theta}{}^M = \frac{-\mu(1+\nu_u)B\Delta m}{3\pi\rho_0(1-\nu_u)r^2}V^I \tag{B15}$$

where $V^I = \pi r_0{}^2$.

APPENDIX C: LINE OF CENTERS OF DILATATION IN A HALF-SPACE

The Green's functions for the half-plane, corresponding to a line of centers of dilatation (or contraction), can be derived from the known solutions for point forces in a half-plane. *Melan* [1932] found the solution for a point force in an elastic half-plane. Using the familiar relationship between elastic constants in plane stress and plane strain, Melan's results can be transformed to the corresponding plane strain solution. For a force per unit length F perpendicular to the free surface located at $x = \zeta$, $y = \xi$ the appropriate Airy stress function $\phi^\perp$ is

$$\phi^\perp = \frac{F}{\pi}\left\{\frac{(y-\xi)(\theta_1+\theta_2)}{2} - \frac{1}{2(1-\nu)} \cdot \left[\frac{\zeta x(\zeta + x)}{r_2{}^2} + \frac{(1-2\nu)}{2}(x-\zeta)\log\frac{r_1}{r_2}\right]\right\} \tag{C1}$$

where

$$r_1{}^2 = (x-\zeta)^2 + (y-\xi)^2 \qquad r_2{}^2 = (x+\zeta)^2 + (y-\xi)^2 \tag{C2}$$

$$\theta_1 = \tan^{-1}[(y-\xi)/(x-\zeta)] \qquad \theta_2 = \tan^{-1}[(y-\xi)/(x+\zeta)] \tag{C3}$$

The complementary stress function for a force parallel to the free surface $\phi^\parallel$ is

$$\phi^\parallel = \frac{F}{\pi}\left\{-(x-\zeta)\frac{(\theta_1+\theta_2)}{2} + \frac{1}{2(1-\nu)} \cdot \left[\frac{\zeta x(y-\xi)}{r_2{}^2} - \frac{(1-2\nu)}{2}(y-\xi)\log\frac{r_1}{r_2}\right]\right\} \tag{C4}$$

The stress function for a center of dilatation is found by differentiating the point-force stress functions with respect to the source location to obtain two orthogonal force dipoles, and then superimposing the orthogonal dipoles [*Love*, 1944, p. 213]. If ϕ is the stress function for the center of dilatation, then

$$\phi = -\left(\frac{\partial\phi^\perp}{\partial\zeta} + \frac{\partial\phi^\parallel}{\partial\xi}\right) \tag{C5}$$

Differentiating (C1) and (C4)

$$\phi = C\left[\log\left(\frac{r_1}{r_2}\right) + \frac{2x(x+\zeta)}{r_2{}^2}\right] \tag{C6}$$

The displacements can be found directly from the stress function by differentiation.

$$u_n(x, y) = \frac{C}{\mu} g_n(x, y, \zeta, \xi) \tag{C7}$$

where

$$g_x = \frac{1}{2}\left\{\frac{x-\zeta}{r_1^2} + \frac{2x - (3-4\nu_u)(x+\zeta)}{r_2^2} - \frac{4x(x+\zeta)^2}{r_2^4}\right\}$$
$$g_y = \frac{1}{2}\left\{\frac{y-\xi}{r_1^2} + \frac{(3-4\nu_u)(y-\xi)}{r_2^2} - \frac{4x(x+\zeta)(y-\xi)}{r_2^4}\right\} \tag{C8}$$

where C is a constant, with units of force, proportional to the source strength. On the free surface ($x = 0$) the displacement functions are

$$g_x(x=0, y) = 2(1-\nu_u)\left[\frac{-\zeta}{\zeta^2 + (y-\xi)^2}\right]$$
$$g_y(x=0, y) = 2(1-\nu_u)\left[\frac{(y-\xi)}{\zeta^2 + (y-\xi)^2}\right] \tag{C9}$$

The stresses due to the centers of dilatation can be found from Hooke's law through equation (17), or directly from the stress function (C6); they are of the form

$$\sigma_{mn} = CG_{mn}(x, y, \zeta, \xi) \qquad m, n = x, y \tag{C10}$$

where the functions G_{mn} are

$$G_{xx} = \frac{(y-\xi)^2 - (x-\zeta)^2}{r_1^4} + \frac{(5x+\zeta)(x+\zeta) - (y-\xi)^2}{r_2^4} - \frac{16x(x+\zeta)(y-\xi)^2}{r_2^6}$$
$$G_{yy} = \frac{(x-\zeta)^2 - (y-\xi)^2}{r_1^4} + \frac{(x+\zeta)(3\zeta - x) - 3(y-\xi)^2}{r_2^4} + \frac{16x(x+\zeta)(y-\xi)^2}{r_2^6} \tag{C11}$$
$$G_{xy} = \frac{-2(y-\xi)(x-\zeta)}{r_1^4} - \frac{2(y-\xi)(3x+\zeta)}{r_2^4} + \frac{16x(x+\zeta)^2(y-\xi)}{r_2^6}$$

The value of the constant C is determined by requiring that as the depth of the source becomes large ($\zeta \to \infty$), the displacements and stresses given by (C8) and (C11) approach those of a localized change of pore fluid in a full-plane. In this limit the terms with r_2 in the denominator tend toward zero. Comparing (C7) and (C8) with (B14) and recalling that $u_r^2 = u_x^2 + u_y^2$, it is clear that

$$C = \frac{\mu B(1+\nu_u)\Delta m}{3\pi\rho_0(1-\nu_u)}\, dV \tag{C12}$$

where for a point center of dilatation the inclusion volume V^I is reduced to the infinitesimal dV.

The displacements due to a point change in fluid mass content in a half-space can now be written from (C7) and (C12) as

$$u_n(x, y) = \frac{(1+\nu_u)B\Delta m(\zeta, \xi)\, dV}{3\pi\rho_0(1-\nu_u)}\, g_n(x, y, \zeta, \xi) \tag{C13}$$

where the g_n are given in (C8).

Acknowledgments. I would like to thank Richard Curtain of the California Division of Oil and Gas for providing valuable data on the Coalinga oil fields, as well as R. Stein, R. F. Yerkes, A. Bartow, D. Eberhart-Phillips, P. Reasenberg, G. Mavko, and E. Roeloffs for stimulating discussion and advice. The manuscript was reviewed by A. McGarr, J. D. Bredehoeft, W. Thatcher, and J. Rudnicki. I am especially grateful to J. Rudnicki for his conscientious review, which presented a more straightforward derivation of the principal results and pointed out an error in the calculated mean stresses.

REFERENCES

Bell, M. L., and A. Nur, Strength changes due to reservoir-induced pore pressure and stresses and application to Lake Oroville, *J. Geophys. Res.*, *83*, 4469–4483, 1978.

Bennett, J. H., and R. W. Sherburne, Preface to the 1983 Coalinga, California earthquakes, *Spec. Publ. Calif. Div. Mines Geol.*, *66*, 1, 1983.

Biot, M. A., General theory of three-dimensional consolidation, *J. Appl. Phys.*, *12*, 155–164, 1941.

Brace, W. F., Permeability of crystalline and argillaceous rocks, *Int. J. Rock Mech. Min. Sci. Geomech. Abstr.*, *17*, 241–251, 1980.

Bull, W. B., Land subsidence due to ground-water withdrawal in the Los Banos-Kettleman City area, 2, Subsidence and compaction of deposits, *U.S. Geol. Surv. Prof. Pap.*, *437-F*, 90 pp., 1975.

California Division of Oil and Gas, *Summary of Operations, California Oil Fields*, vol. 31–67, Sacramento, 1945–1981.

California Division of Oil and Gas, *California Oil and Gas Fields*, vol. 1, *North and East Central California*, Sacramento, 1973.

Carslaw, A. R., and C. J. Jaeger, *Conduction of Heat in Solids*, Oxford at the Clarendon Press, London, 1959.

Chinnery, M. A., Theoretical fault models, in *A Symposium on Processes in the Focal Region*, edited by K. Kasahara and A. E. Stevens, pp. 211–223, Dominion Observatory, Ottawa, 1969.

Clark, M., K. Harms, J. Lienkaemper, J. Perkins, M. Rymer, and R. Sharp, The search for surface faulting, *U.S. Geol. Surv. Open File Rep.*, *83-511*, 8–11, 1983.

Conservation Committee of California Oil Producers, Annual review of California oil and gas production, Los Angeles, Calif., 1931–1984.

Dundurs, J., and D. L. Guell, Center of dilatation and thermal stresses in joined elastic half-spaces, in *Developments in Theoretical and Applied Mechanics*, vol. 2, *Proceedings Second Southeastern Conference Theoretical and Applied Mechanics, Atlanta, March 5–6, 1964*, edited by W. A. Shaw, pp. 199–211, Pergamon, New York, 1965.

Eaton, J., R. Cockerham, and F. Lester, Study of the May 2, 1983 Coalinga earthquake and its aftershock, based on the USGS seismic network in northern California, in *Spec. Publ. Calif. Div. Mines Geol.*, *66*, 261–273, 1983.

Eshelby, J. D., The determination of the elastic field of an ellipsoidal inclusion and related problems, *Proc. R. Soc. London, Ser. A*, *241*, 376–396, 1957.

Fowkes, E. S., *An Educational Guidebook to the Geologic Resources of the Coalinga District, California*, 260 pp., West Hills College, Coalinga, Calif., 1982.

Gambolati, G., A three-dimensional model to compute land subsidence, *Bull. Int. Assoc. Hydrol. Sci.*, *17*, 219–226, 1972.

Gambolati, G., Second-order theory of flow in three-dimensional deforming media, *Water Resour. Res.*, *10*, 1217–1228, 1974.

Gambolati, G., and R. A. Freeze, Mathematical simulation of the subsidence of Venice, *Water Resour. Res.*, *9*, 721–733, 1973.

Geertsma, J., Problems of rock mechanics in petroleum production engineering, *Proc. Congr. Int. Soc. Rock Mech.*, *1st*, 585–594, 1966.

Healy, J. H., W. W. Rubey, D. T. Griggs, and C. B. Raleigh, The Denver earthquakes, *Science*, *161*, 1301–1310, 1968.

Holdahl, S. K., A model of temperature stratification for correction of leveling refraction, *Bull. Geod.*, *55*, 231–249, 1981.

Kovach, R. L., Source mechanisms for Wilmington oil field, California, subsidence earthquakes, *Bull. Seismol. Soc. Am.*, *64*, 699–711, 1974.

Love, A. E. H., *A Treatise on the Mathematical Theory of Elasticity*, 4th ed., 643 pp., Dover, New York, 1944.

Melan, E., Der Spannungszustand der durch eine einzelkraft im innern beanspruchten halbscheibe, *Angew. Math. Mech.*, *12*, 343–346, 1932. (Correction, *Z. Angew. Math. Mech.*, *20*, 368, 1940.)

Pratt, W. E., and D. W. Johnson, Local subsidence of the Goose Creek oil field, *J. Geol.*, *34*, 577–590, 1926.

Prokopovich, N. P., and D. C. Magleby, Land subsidence in Pleasant

Valley area, Fresno County, Calif., *J. Am. Water Works Assoc., 60*, 413–424, 1968.

Raleigh, C. B., J. H. Healy, and J. D. Bredehoeft, Faulting and crustal stress at Rangely, Colorado, in *Flow and Fracture of Rocks, Geophys. Monogr. Ser.*, vol. 16, edited by H. C. Heard, I. Y. Borg, N. L. Carter, and C. B. Raleigh, pp. 275–284, AGU, Washington, D. C., 1972.

Raleigh, C. B., J. H. Healy, and J. D. Bredehoeft, An experiment in earthquake control at Rangely, Colorado, *Science, 191*, 1230–1237, 1976.

Reasenberg, P., D. Eberhart-Phillips, and P. Segall, Preliminary views of the aftershock distribution, *U.S. Geolog. Surv. Open File Rep., 83-511*, 27–37, 1983.

Rice, J. R., and M. C. Cleary, Some basic stress diffusion solutions for fluid-saturated elastic porous media with compressible constitutents, *Rev. Geophys., 14*, 227–241, 1976.

Rymer, M. J., K. K. Harms, M. M. Clark, and J. J. Lienkaemper, Surface faulting associated with an aftershock of the May 2, 1983 Coalinga, California earthquake, *Eos Trans. AGU, 64*, 748, 1983.

Safai, N. M., and G. Pinder, Vertical and horizontal land deformation due to fluid withdrawal, *Int. J. Numer. Anal. Methods Geomech., 4*, 131–142, 1980.

Simpson, D. W., Seismicity changes associated with reservoir loading, *Eng. Geol., 10*, 123–150, 1976.

Stacey, F. D., *Physics of the Earth*, 324 pp., John Wiley, 1969.

Stein, R. S., Reverse slip on a buried fault during the 2 May 1983 Coalinga earthquake: Evidence from geodetic elevation changes, *Spec. Publ. Calif. Div. Mines Geol., 66*, 151–163, 1983.

Wentworth, C. M., M. C. Blake, Jr., D. L. Jones, A. W. Walter, and M. D. Zoback, Tectonic wedging associated with emplacement of the Franciscan assemblage, California coast ranges, in *Franciscan Geology of Northern California*, edited by M. C. Blake, Jr., pp. 163–173, Society of Economic Paleontologists and Mineralogists, Pacific Section, Los Angeles, Calif., 1984.

Yerkes, R. F., and R. O. Castle, Seismicity and faulting attributable to fluid extraction, *Eng. Geol., 10*, 151–167, 1976.

P. Segall, U.S. Geological Survey, 345 Middlefield Road, MS/77, Menlo Park, CA 94025.

(Received May 17, 1984;
revised March 21, 1985;
accepted March 23, 1985.)